

Surface s -wave superconductivity for oxide-terminated infinite-layer nickelates

Xianxin Wu,^{1,2,*} Kun Jiang,² Domenico Di Sante,³ Werner Hanke,³ A. P. Schnyder,¹ Jiangping Hu,^{2,4} and Ronny Thomale³

¹Max-Planck-Institut für Festkörperforschung, Heisenbergstrasse 1, D-70569 Stuttgart, Germany

²Beijing National Laboratory for Condensed Matter Physics,
and Institute of Physics, Chinese Academy of Sciences, Beijing 100190, China

³Institut für Theoretische Physik und Astrophysik and Würzburg-Dresden Cluster of Excellence *ct.qmat*,
Universität Würzburg, Am Hubland Campus Süd, Würzburg 97074, Germany

⁴CAS Center of Excellence in Topological Quantum Computation and Kavli Institute of Theoretical Sciences,
University of Chinese Academy of Sciences, Beijing 100190, China

(Dated: September 1, 2020)

We analyze the electronic structure of different surface terminations for infinite-layer nickelates. Surface NiO₂ layers are found to be buckled, in contrast to planar bulk layers. While the rare-earth terminated surface fermiology is similar to the bulk limit of the nickelates, the NiO₂ terminated surface band structure is significantly altered, originating from the effect of absence of rare-earth atoms on the crystal field splitting. Contrary to the bulk Fermi surfaces, there are two Ni-3d Fermi pockets, giving rise to enhanced spectral weight around the \bar{M} point in the surface Brillouin zone. From a strong-coupling analysis, we obtain dominant extended s -wave superconductivity for the surface layer, as opposed to d -wave for the bulk. This finding distinguishes the nickelates from isostructural cuprates, where the analogous surface pairing mechanism is less pronounced. Our results are consistent with region-dependent gap structures revealed in recent STM measurements and provide an ansatz to interpret experimental data of surface-sensitive measurements on the infinite-layer nickelates.

Introduction – The recent discovery of superconductivity in Sr-doped infinite-layer rare-earth nickelates (Nd,Pr)NiO₂ [1, 2] has expanded the range of material classes that are promising hosts for unconventional superconductivity. Starting from the cuprates for which overwhelming experimental evidence is consistent with a d -wave order parameter [3], iron pnictides are assumed to predominantly exhibit unconventional s -wave order. There, the s -wave superconducting order is microscopically preferred by the multi-pocket fermiology [4, 5]. Even though the field is still too young to draw concise connections to more established unconventional superconductors, the infinite-layer nickelates seemingly present themselves as a hybrid between cuprates and pnictides: while the NiO₂ layers share close structural similarity to the cuprates, their multi-orbital nature [6] appears more related to the iron pnictides.

The band structure of RNiO₂ (R=rare earth) crystals is of 3D dispersive type with a dominant Ni $d_{x^2-y^2}$ hole band and two R $5d$ electron bands [7–11] or a R d_{z^2} electron band and an interstitial s electron band [12–14]. The theoretical understanding of the correlated electronic structures and pairing states of the nickelates remains controversial so far. Because of the large charge-transfer energy between the Ni-3d and O-2p states in RNiO₂, the system is suggested to be in the Hubbard regime, distinct from the charge-transfer nature of cuprates [6, 15, 16]. Recent comprehensive dynamical mean-field theory (DMFT) and GW calculations, however, suggest that both RNiO₂ and CaCuO₂ are charge-transfer materials [17–19]. Moreover, the multi-orbital nature is genuine in both undoped and hole-doped NdNiO₂ [6, 20], and Hund’s metal physics is likewise argued to be relevant [21, 22]. With respect to pairing symmetry, the bulk phase is expected to show a robust d -wave pairing, similar to the cuprates [10, 11, 23] in a predominantly electronically mediated mechanism. Within a $K - t - J$ model [24], the

pairing state is found to be $(d + is)$ -wave in the small doping region and changes to a d -wave pairing at larger doping [25].

Until today, the complicated sample growth has prevented a better experimental grasp of the detailed properties of infinite-layer nickelates. Recent experiments revealed an intriguing double-peak T_c dome and weakly insulating behaviors on both sides of the dome [26, 27]. It is challenging to perform and interpret surface-sensitive spectroscopy on the nickelates, such as stemming from angle-resolved photo emission (ARPES), which has not yet been reported, or scanning tunneling microscopy (STM) [28]. These experiments would always be particularly sensitive to the electronic structure near the surface, which was likewise observed in cuprates and iron pnictides [29–31]. Due to the strong hybridization between rare-earth atoms and NiO₂ layers [12, 14], the electronic structure of surface NiO₂ layers can be dramatically distinct from bulk layers. Moreover, the mechanism behind the recent observation of mixed s -wave and d -wave gap signatures on a rough surface in STM is still unresolved [28]. Therefore, the surface modelling of the infinite-layer nickelates can be helpful for a better understanding of the present and future experimental evidences on electronic structure and superconductivity.

In this Letter, we analyse the electronic structure of different surface terminations for infinite-layer nickelates. From the given layered structure and assuming the clean material limit, two different terminations with either a final rare earth layer or NiO₂ layer have to be investigated. From an *ab initio* treatment of the two different structures, we obtain effective surface fermiologies for both terminations, which we then further investigate with respect to the onset of superconductivity. The rare-earth termination is dominated by a single Ni-type $d_{x^2-y^2}$ Fermi pocket with slight electron doping [Fig.1 (b)]. This makes the surface band structure appear similar to the dominant bulk bands, suggesting the onset of d -wave super-

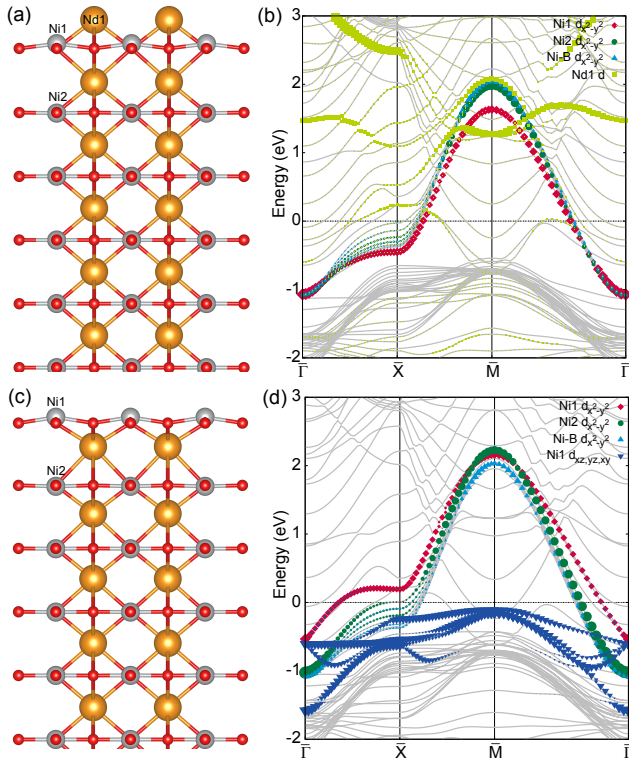


FIG. 1. Crystal structures for (a) the Nd terminated surface and (c) the NiO₂ terminated surface of NdNiO₂. (b) and (d) are the corresponding orbital resolved band structures. "Ni-B" denotes the bulk Ni atom.

conductivity. The NiO₂ termination, however, effectively appears significantly more hole doped than the bulk bands [Fig. 1(d)]. Owing to the modified crystal-field splitting effect due to absence of the upper rare-earth atoms, a second Ni-type Fermi pocket appears around the M point of the surface Brillouin zone, suggesting a multi-orbital nature. Based on a mean-field t - J model analysis we find that this two-pocket fermiology naturally favors an extended s -wave superconducting order parameter. It yields a full gap along with a sign change between the two Fermi pockets. We further show that the strong effect arising from the surface termination is specific to the infinite-layer nickelate superconductors, while the isostructural cuprates do not exhibit such a strong propensity. Moreover, we analyze the scenario of Josephson coupling between an s -wave surface and a d -wave sub-surface state or rough surface islands of different termination, which in the clean limit could yield $(s + id)$ -wave pairing in order to maximize the condensation energy within the two layers. In the light of these findings, we give an interpretation of recent STM measurements on rough NdNiO₂ surfaces with admixed regions of rare earth and NiO₂ terminations. Furthermore, we outline experiments, such as, reflectivity measurements to investigate possible Josephson plasma modes or Kerr spectroscopy to detect time-reversal symmetry breaking without parity breaking in a disordered $s + id$ state.

Electronic structures of the two surface terminations – For

NdNiO₂, there are two kinds of surface terminations, namely, Nd terminated and NiO₂ terminated surfaces, as shown in Fig. 1(a) and 1(c), respectively. The electronic structure of the NdNiO₂/SrTiO₃ interface have been theoretically studied [32–34]. In our calculations we modeled these surfaces using slabs of eight NiO₂ layers and eight or nine Nd layers plus a vacuum layer of 15 Å. In the relaxation, the bottom five layers are fixed while the others are allowed to move freely. The details of calculations can be found in Sec. I of the supplementary materials (SM). After relaxation, one prominent feature is that the surface NiO₂ layers are not planar but buckled in both terminations, distinct from bulk layers, which is in response to the internal electric field build-up in the polar slabs [33, 34].

For the Nd terminated surface, the Ni height with respect to the oxygen plane is smaller of about 0.25 Å, owing to the hybridization between top Nd and oxygen atoms. The orbitally resolved band structure of Fig. 1(b) shows that the Ni $d_{x^2-y^2}$ band of the top NiO₂ layer is slightly electron-doped, resembling the bulk band in the $k_z = 0$ plane. The bands in gray lines crossing the Fermi level around $\bar{\Gamma}$ and \bar{M} points are attributed to bulk Nd d orbitals [7–11]. Similar to bulk layers, other Ni d orbitals are located far below the Fermi level and surface Nd atoms have some contributions to the Fermi surfaces.

For the NiO₂ terminated surface, the Ni height with respect to the oxygen plane is larger and about 0.30 Å in the surface layer. The underlying Nd layer further moves closer to the top NiO₂ layer with a vertical separation of 1.23 Å and couples strongly with oxygen atoms (Fig. 1(c)). The corresponding orbitally resolved band structure is displayed in Fig. 1(d). We find that the $d_{x^2-y^2}$ band of the surface NiO₂ (red diamonds) is heavily hole-doped compared with bulk NiO₂ layers (blue up-triangles) due to the absence of the charge reservoir layer, i.e., rare-earth atoms. Moreover, it also significantly affects the crystal field splitting and pushes upwards Ni $d_{xz/yz}$ and d_{xy} orbitals. The onsite energies of the $d_{xz/yz}$ and the d_{xy} orbitals relative to the $d_{x^2-y^2}$ orbital on the surface layer increase by 0.45 and 0.16 eV, respectively, compared with bulk layers. Therefore, the Ni d_{xy} , $d_{xz/yz}$ orbitals have strong hybridizations with $d_{x^2-y^2}$ orbitals near the Fermi level and their bands are located just slightly below the Fermi level, especially around the \bar{M} point. Actually, these bands cross the Fermi level without surface atomic relaxation (see Sec. I of SM). Without external doping, there is only a small electron pocket around the $\bar{\Gamma}$ point for the surface NiO₂ layer. In experiments, superconductivity was achieved by hole doping, introduced by the substitution of Nd by Sr[1, 2]. Therefore, the multi-orbital nature is expected to be relevant for the hole-doped NiO₂ surface; this is distinct from bulk NiO₂ layers, where only Ni $d_{x^2-y^2}$ orbital plays an essential role [10, 11].

As the rare-earth atoms are not ionic charge carriers and couple strongly to NiO₂ layers in infinite-layer RNiO₂, the multi-orbital nature is a unique feature on its NiO₂-terminated surface. To demonstrate this, we also performed similar calculations for their cuprate analog CaCuO₂ whose band struc-

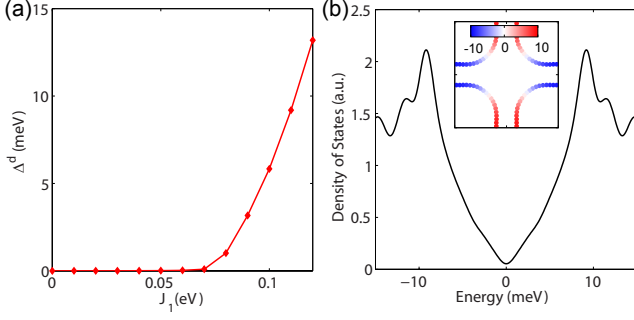


FIG. 2. (a) The absolute value of d -wave gap as a function of the exchange coupling parameter J_1 for the Nd terminated surface of $\text{Nd}_{0.8}\text{Sr}_{0.2}\text{NiO}_2$. (b) Density of states of the d -wave pairing state at the Nd terminated surface for $J_1 = 0.1$ eV. The inset shows the momentum dependence of the gap along the Fermi surface in units of meV.

tures for the two terminations are provided in the Sec. II of SM. There, for both terminations, only the Cu $d_{x^2-y^2}$ orbital of the surface CuO_2 layer dominates near the Fermi level, while other Cu d orbitals are well below the Fermi level in accordance with its charge-transfer nature.

Pairing states for surface layers – For the bulk system, a robust $d_{x^2-y^2}$ -wave pairing is found for $\text{Nd}_{1-x}\text{Sr}_x\text{NiO}_2$, dominantly contributed by the Ni $d_{x^2-y^2}$ -orbital Fermi surface [10, 11]. The surface layers can favor distinct pairing states from the bulk, owing to their different carrier dopings and electronic structures. For the Nd terminated surface, despite slight electron doping, the Fermiology of surface layer is close to that of a bulk layer for the $k_z = 0$ plane. Therefore, the surface layer is expected to favor a $d_{x^2-y^2}$ pairing as well. We perform numerical calculations to verify it: we first construct the one band tight-binding (TB) model (Sec. III of SM) to describe the electronic structure of the surface NiO_2 layer and then study the pairing within a similar t-J model as Ref. [11]. Fig.2(a) displays the d -wave gap as a function of the exchange parameter and the s -wave gap vanishes, indicating that the d -wave pairing is dominant. The corresponding density of states (DOS), shown in Fig.2(b), exhibits a V-shaped gap structure, similar to bulk NiO_2 layers or typical cuprates.

For the NiO_2 terminated surface, however, other d orbitals than $d_{x^2-y^2}$ can likewise contribute to the fermiology of the top NiO_2 layer, which may result in a change of pairing symmetry. We first study the multi-orbital TB model for the distorted NiO_2 layers with heavy hole doping and introduce the operator $\psi_{\mathbf{k}\sigma}^\dagger = [c_{1\sigma}^\dagger(\mathbf{k}), c_{2\sigma}^\dagger(\mathbf{k}), c_{3\sigma}^\dagger(\mathbf{k}), c_{4\sigma}^\dagger(\mathbf{k}), c_{5\sigma}^\dagger(\mathbf{k})]$, where $c_{\alpha\sigma}^\dagger(\mathbf{k})$ is a Fermionic creation operator with σ and α denoting spin and orbital indices, respectively. The orbital index $\alpha = 1, 2, 3, 4, 5$ represents the Ni $d_{x^2-y^2}$ for 1, d_{xy} for 2, d_{xz} for 3, d_{yz} for 4 and d_{z^2} for 5, respectively. The TB Hamiltonian can be written as,

$$H_0 = \sum_{\mathbf{k}\sigma} \psi_{\mathbf{k}\sigma}^\dagger (h(\mathbf{k}) - \mu) \psi_{\mathbf{k}\sigma}. \quad (1)$$

The matrix elements in the Hamiltonian $h(\mathbf{k})$ matrix are given

in the Sec. III of SM. The orbitally resolved band structure from the above TB model, showing good agreement with DFT calculations (Sec. III of SM), is displayed in Fig.3(a). In experiments, a superconducting dome was found in $\text{Nd}_{1-x}\text{Sr}_x\text{NiO}_2$ for $0.12 \leq x \leq 0.25$ [26]. Assuming that charge transfer from (Nd,Sr) layers to NiO_2 layers is inversely proportional to their separations, the hole doping of surface NiO_2 layer is estimated to be $0.08 \leq \delta \leq 0.16$. Within this doping level, there are an electron pocket around the $\bar{\Gamma}$ point and a hole pocket around the \bar{M} point, attributed to Ni $d_{x^2-y^2}$, d_{xy} and $d_{xz/yz}$ orbitals. These Fermi surfaces can also be reproduced in $\text{Nd}_{0.8}\text{Sr}_{0.2}\text{NiO}_2$ in first-principles calculations (Sec. I of SM). Since the bands around the \bar{M} point are flat, the corresponding hole pocket has a large DOS. Representative Fermi surfaces with a hole doping $\delta = 0.12$ (for $\text{Nd}_{0.8}\text{Sr}_{0.2}\text{NiO}_2$) are shown in Fig.3(b), suggesting that the multi-orbital nature is one prominent feature for surface NiO_2 layers.

Due to the appearance of the hole pocket around \bar{M} with an enhanced spectral weight, distinct from over-doped cuprates, and in order to account for the multi-orbital nature of the surface NiO_2 layers, we adopt a multi-orbital t-J model to study pairing propensities. Similar to iron-based superconductors [35, 36], we consider for the surface NiO_2 layers in-plane antiferromagnetic coupling between the Ni spins,

$$H_J = \sum_{\langle ij \rangle \alpha} J_{ij}^\alpha (\mathbf{S}_{i\alpha} \mathbf{S}_{j\alpha} - \frac{1}{4} n_{i\alpha} n_{j\alpha}) \quad (2)$$

where $\mathbf{S}_{i\alpha} = \frac{1}{2} c_{i\alpha\sigma}^\dagger \boldsymbol{\sigma}_{\sigma\sigma'} c_{i\alpha\sigma'}$ is the local spin operator and $n_{i\alpha}$ is the local density operator for Ni α orbital ($\alpha = x^2 - y^2, xy, xz, yz, z^2$). $\langle ij \rangle$ denotes the in-plane nearest neighbors and the in-plane coupling is $J_x^\alpha = J_y^\alpha = J_1^\alpha$. By performing the Fourier transformation, H_J in momentum space reads

$$H_J = \sum_{\alpha\mathbf{k},\mathbf{k}'} V_{\mathbf{k},\mathbf{k}'}^\alpha c_{\mathbf{k}\alpha\uparrow}^\dagger c_{-\mathbf{k}\alpha\downarrow}^\dagger c_{-\mathbf{k}'\alpha\downarrow} c_{\mathbf{k}'\alpha\uparrow}, \quad (3)$$

with $V_{\mathbf{k},\mathbf{k}'}^\alpha = -\frac{2J_1^\alpha}{N} \sum_{\pm} (\cos k_x \pm \cos k_y)(\cos k'_x \pm \cos k'_y)$ and N being the number of lattice sites. Here we investigate the pairing state for the doped system and neglect the no-double-occupancy constraint on this t-J model and then perform a mean-field decoupling (details can be found in Sec. IV of SM). In the calculations, we only consider the intraorbital pairing and neglect inter-orbital pairing, as the orbital mixture on Fermi surfaces is not strong. The orbital dependent gap is defined as $\Delta_\alpha^{s/d} = -\frac{2J_1^\alpha}{N} \sum_{\mathbf{k}'} \langle c_{-\mathbf{k}'\alpha\downarrow} c_{\mathbf{k}'\alpha\uparrow} \rangle (\cos k'_x \pm \cos k'_y)$ and we further introduce $\Delta_{31}^{s/d} = \frac{1}{2} (\Delta_3^s \pm \Delta_4^s + \Delta_3^d \mp \Delta_4^d)$ and $\Delta_{32}^{s/d} = \frac{1}{2} (\Delta_3^s \pm \Delta_4^s - \Delta_3^d \pm \Delta_4^d)$ for $d_{xz/yz}$ orbitals. The obtained gaps as a function of exchange coupling parameters at $\delta = 0.12$ are shown in Fig.3(c) and the doping dependent gaps are given in Sec. IV of SM. We find that the extended s -wave pairing is always dominant within the estimated hole doping region, and that the gap of d_{xy} orbital is much larger than other orbitals, originating from its enhanced DOS around \bar{M} .

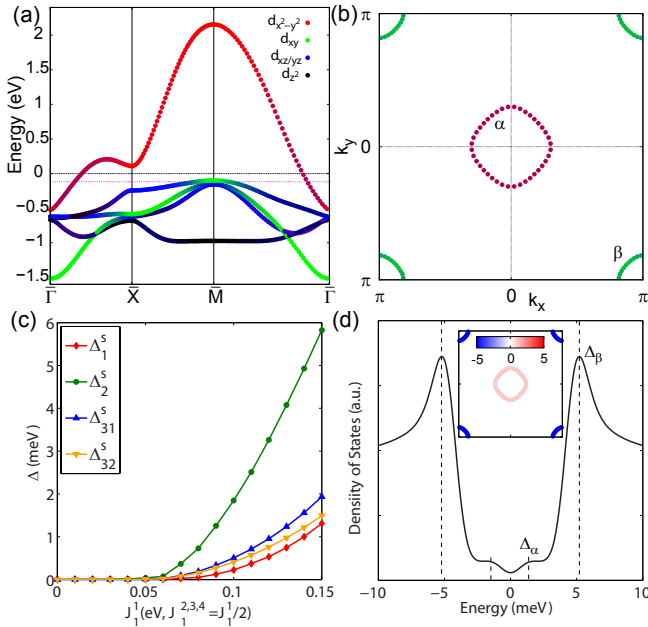


FIG. 3. (a) Orbitaly resolved band structure of the TB model for the surface NiO₂ layer. The pink dashed line denotes the chemical potential for hole doping $\delta = 0.12$. (b) Representative Fermi surfaces with orbital characters for the hole-doped surface NiO₂ layer of Nd_{0.8}Sr_{0.2}NiO₂ (hole doping level is $\delta = 0.12$). (c) Orbital dependent superconducting gaps as a function of exchange coupling parameters for $\delta = 0.12$ with $J_1^{2,3,4} = J_1^1/2$. (d) Density of states of the extended *s*-wave pairing state in the NiO₂ surface layer for $\delta = 0.12$ and $J_1^1 = 0.12$ eV. The inset shows the momentum dependence of the gap along the FSs in units of meV.

Moreover, as displayed in the inset of Fig.3(d), there is a sign change in the gap function between the electron pocket around $\bar{\Gamma}$ and the hole pocket around \bar{M} , in analogy to s_{\pm} pairing in iron based superconductors [5] and overdoped CuO₂ monolayers [37]. The corresponding DOS in Fig.3(d) exhibits a general U-shaped structure and two-gap feature.

Termination-dependent gap structures – In experiments, two terminations are expected to be randomly distributed on the surface. In the (Sr,Nd) terminated surface, a V-shaped gap is expected in the tunneling spectrum of STM measurements. For the NiO₂ terminated surface, however, the surface NiO₂ layer has s_{\pm} -wave pairing, inducing a U-shaped gap. In the domain wall between two kinds of terminations, shown in Fig.4(a), zero-energy Andreev flat bands will appear in the [11] or $[1\bar{1}]$ direction, inducing a sharp zero-bias peak in the local DOS of Fig.4(b). Note that the extensive ground-state degeneracy of the Andreev flat bands is thermodynamically unstable. I.e., at low enough temperatures it will be lifted by residual interactions, which induce a symmetry-broken state at the edge, e.g., $(d + is)$ -wave pairing at the edge, or possibly edge magnetism [38, 39]. This should be observable in experiments in terms of a splitting of the zero-bias peak at low temperatures.

As the surface NiO₂ layer has s_{\pm} -wave pairing and the bulk

NiO₂ layer favors a $d_{x^2-y^2}$ -wave pairing, the coupling between them introduces a Josephson junction along the *c* axis. While this scenario is not what is given in current experiments, one might reach it in future samples due to the enhancement of synthesis quality. Generally, the free energy of a Josephson junction [40–42] can be written as,

$$F = F_0 - g_1 \cos \Delta \phi + g_2 \cos 2 \Delta \phi, \quad (4)$$

where $\Delta \phi$ is the phase difference between the two superconducting order parameters. The first term is independent of the phase difference and the second and third terms are the first order and second order Josephson couplings, respectively. Usually, the conventional Josephson coupling g_1 is much larger than g_2 . However, in our case, as the two superconducting orders belong to two different irreducible representations, g_1 should vanish. Therefore, the remaining second order Josephson coupling g_2 will lead to $\Delta \phi = \pm \frac{\pi}{2}$ by minimizing the free energy, forming an $s_{\pm} \pm id_{x^2-y^2}$ pairing state depending on the sign of g_2 . We perform calculations with a t-J model by including both Hamiltonians of surface and bulk NiO₂ layers and their hybridizations (details in Sec. IV of SM), and find that the time-reversal-symmetry breaking $s_{\pm} - id_{x^2-y^2}$ pairing state is energetically more favorable. The corresponding DOS is shown in Fig.4(c), where the gap is generally V-shaped enriched with multiple-gap features. In such a state, supercurrent can be induced near a nonmagnetic impurity and the corners of a square sample, which may be detected by using SQUID [43].

Recent STM measurements seem to reveal an *s*-wave gap and a *d*-wave gap depending on the probed region and a mixture of them in some cases [44]. In contrast to the explanation given in Ref. [44], we do not believe that this observation can be explained by orbitally selective pairing, where the Ni $d_{x^2-y^2}$ -derived Fermi surface has a *d*-wave superconducting gap while Nd d_{xy,z^2} -derived Fermi surfaces have an *s*-wave superconducting gap [44]. As the hybridization between Ni $d_{x^2-y^2}$ and Nd d_{xy,z^2} orbitals is strong, these Fermi surfaces will naturally have superconducting gaps with the same symmetry, but different gap sizes. Instead the scenario of different terminations presents on a rough surface seems consistent with the experimental measurements: following our explanation there should be a *d*-wave gap for the (Nd,Sr)-terminated surface and an *s*-wave gap for the NiO₂-terminated surface; further including the coupling between surface and bulk NiO₂ layers, a mixture of those two superconducting order appears natural to occur for a partially NiO₂-terminated surface.

Conclusion – We investigated the electronic structures for different surface terminations in infinite-layer nickelates and find that the surface NiO₂ layer has a buckled structure and differs from the bulk layer in terms of charge doping. The rare earth terminated surface Fermiology is similar to the bulk albeit with a moderate electron doping. For the NiO₂ terminated surface, however, the absence of rare-earth atoms significantly affects the crystal field splitting and pushes upwards the Ni $d_{xz/yz}$ and d_{xy} orbitals. Consequently, the surface layer is not only heavily hole-doped but also develops an ad-

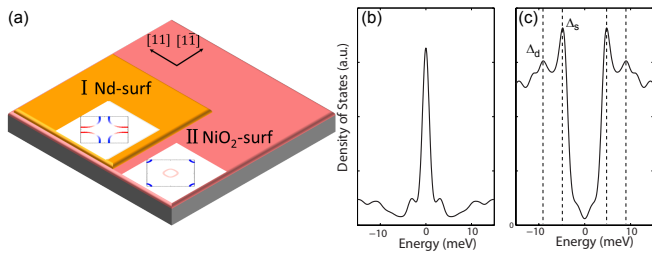


FIG. 4. (a) Schematic for the different surface terminations of NdNiO₂. (b) DOS at the domain boundary between Nd-terminated and NiO₂-terminated surfaces along the [11] or [1̄1] direction. (c) DOS for the $s_{\pm} - id_{x^2-y^2}$ pairing state including the coupling between surface and bulk NiO₂ layers.

ditional electron pocket around the \bar{M} point besides the hole pocket around $\bar{\Gamma}$, derived from d_{xy} and d_{xz}/yz orbitals. From a strong coupling analysis, we find that this two-pocket Fermiology naturally favors an s_{\pm} -wave pairing, in analogy to iron based superconductors. Further including the bulk $d_{x^2-y^2}$ -wave pairing, the second order Josephson coupling induces a $s_{\pm} - id_{x^2-y^2}$ pairing state in the system. Our results seem to be in line with recent experimental observations of both s -wave gap and d -wave gap signatures. Our finding provide a starting point for interpreting surface-sensitive spectroscopy data in future experiments on infinite-layer nickelates, such as ARPES or optical spectroscopy, including Kerr measurements to possibly track down the time-reversal symmetry breaking from any kind of surface $s + id$ pairing.

Acknowledgments— We thank Yujie Sun for helpful discussions. This work is funded by the Deutsche Forschungsgemeinschaft (DFG, German Research Foundation) through Project-ID 258499086 - SFB 1170 and through the Würzburg-Dresden Cluster of Excellence on Complexity and Topology in Quantum Matter-ct.qmat Project-ID 390858490 - EXC 2147. J.P.Hu was supported by the Ministry of Science and Technology of China 973 program (No. 2017YFA0303100), National Science Foundation of China (Grant No. NSFC11888101), and the Strategic Priority Research Program of CAS (Grant No.XDB28000000).

Note added: We recently became aware of an independent work about nickelate thin films grown on SrTiO₃ substrate [45], where the surface distortions and the band structure of NiO₂ terminated surface are consistent with our paper.

* xianxinwu@gmail.com

- [1] D. Li, K. Lee, B. Y. Wang, M. Osada, S. Crossley, H. R. Lee, Y. Cui, Y. Hikita, and H. Y. Hwang, *Nature* **572**, 624 (2019).
- [2] M. Osada, B. Y. Wang, B. H. Goodge, K. Lee, H. Yoon, K. Sakuma, D. Li, M. Miura, L. F. Kourkoutis, and H. Y. Hwang, *Nano letters* **20**, 5735 (2020).
- [3] C. Tsuei and J. Kirtley, *Physica C: Superconductivity* **341-348**, 1625 (2000).
- [4] G. R. Stewart, *Rev. Mod. Phys.* **83**, 1589 (2011).

- [5] P. J. Hirschfeld, M. M. Korshunov, and I. I. Mazin, *Reports on Progress in Physics* **74**, 124508 (2011).
- [6] B. H. Goodge, D. Li, M. Osada, B. Y. Wang, K. Lee, G. A. Sawatzky, H. Y. Hwang, and L. F. Kourkoutis, arXiv e-prints, arXiv:2005.02847 (2020), arXiv:2005.02847 [cond-mat.supr-con].
- [7] K.-W. Lee and W. E. Pickett, *Phys. Rev. B* **70**, 165109 (2004).
- [8] A. S. Botana and M. R. Norman, *Phys. Rev. X* **10**, 011024 (2020).
- [9] M. Hepting, D. Li, C. J. Jia, H. Lu, E. Paris, Y. Tseng, X. Feng, M. Osada, E. Been, Y. Hikita, Y. D. Chuang, Z. Hussain, K. J. Zhou, A. Nag, M. Garcia-Fernandez, M. Rossi, H. Y. Huang, D. J. Huang, Z. X. Shen, T. Schmitt, H. Y. Hwang, B. Moritz, J. Zaenen, T. P. Devereaux, and W. S. Lee, *Nature Materials* **19**, 381 (2020).
- [10] H. Sakakibara, H. Usui, K. Suzuki, T. Kotani, H. Aoki, and K. Kuroki, (2019), arXiv:1909.00060.
- [11] X. Wu, D. Di Sante, T. Schwemmer, W. Hanke, H. Y. Hwang, S. Raghu, and R. Thomale, *Phys. Rev. B* **101**, 060504 (2020).
- [12] Y. Nomura, M. Hirayama, T. Tadano, Y. Yoshimoto, K. Nakamura, and R. Arita, *Phys. Rev. B* **100**, 205138 (2019).
- [13] J. Gao, Z. Wang, C. Fang, and H. Weng, arXiv e-prints, arXiv:1909.04657 (2019), arXiv:1909.04657 [cond-mat.mtrl-sci].
- [14] Y. Gu, S. Zhu, X. Wang, J. Hu, and H. Chen, *Communications Physics* **3**, 84 (2020).
- [15] M. Jiang, M. Berciu, and G. A. Sawatzky, *Phys. Rev. Lett.* **124**, 207004 (2020).
- [16] F. Lechermann, *Phys. Rev. B* **101**, 081110 (2020).
- [17] J. Karp, A. S. Botana, M. R. Norman, H. Park, M. Zingl, and A. Millis, *Phys. Rev. X* **10**, 021061 (2020).
- [18] V. Olevano, F. Bernardini, X. Blase, and A. Cano, *Phys. Rev. B* **101**, 161102 (2020).
- [19] D. Di Sante, X. Wu, W. Hanke, and R. Thomale, (To be published) (2020).
- [20] F. Petocchi, V. Christiansson, F. Nilsson, F. Aryasetiawan, and P. Werner, arXiv e-prints, arXiv:2006.00394 (2020), arXiv:2006.00394 [cond-mat.str-el].
- [21] Y. Wang, C. J. Kang, H. Miao, and G. Kotliar, arXiv e-prints, arXiv:2006.15305 (2020), arXiv:2006.15305 [cond-mat.str-el].
- [22] B. Kang, C. Melnick, P. Semon, G. Kotliar, and S. Choi, arXiv e-prints, arXiv:2007.14610 (2020), arXiv:2007.14610 [cond-mat.str-el].
- [23] L.-H. Hu and C. Wu, *Phys. Rev. Research* **1**, 032046 (2019).
- [24] G.-M. Zhang, Y.-f. Yang, and F.-C. Zhang, *Phys. Rev. B* **101**, 020501 (2020).
- [25] Z. Wang, G.-M. Zhang, Y.-f. Yang, and F.-C. Zhang, arXiv e-prints, arXiv:2006.15928 (2020), arXiv:2006.15928 [cond-mat.supr-con].
- [26] D. Li, B. Y. Wang, K. Lee, S. P. Harvey, M. Osada, B. H. Goodge, L. F. Kourkoutis, and H. Y. Hwang, *Phys. Rev. Lett.* **125**, 027001 (2020).
- [27] S. Zeng, C. Sin Tang, X. Yin, C. Li, Z. Huang, J. Hu, W. Liu, G. J. Omar, H. Jani, Z. Shih Lim, K. Han, D. Wan, P. Yang, A. T. S. Wee, and A. Ariando, arXiv e-prints, arXiv:2004.11281 (2020), arXiv:2004.11281 [cond-mat.supr-con].
- [28] Q. Gu, Y. Li, S. Wan, H. Li, W. Guo, H. Yang, Q. Li, X. Zhu, X. Pan, Y. Nie, and H.-H. Wen, (2020), arXiv:2006.13123.
- [29] Y.-F. Lv, W.-L. Wang, J.-P. Peng, H. Ding, Y. Wang, L. Wang, K. He, S.-H. Ji, R. Zhong, J. Schneeloch, G.-D. Gu, C.-L. Song, X.-C. Ma, and Q.-K. Xue, *Phys. Rev. Lett.* **115**, 237002 (2015).
- [30] Y. Zhong, Y. Wang, S. Han, Y.-F. Lv, W.-L. Wang, D. Zhang, H. Ding, Y.-M. Zhang, L. Wang, K. He, R. Zhong, J. A. Schneeloch,

- loch, G.-D. Gu, C.-L. Song, X.-C. Ma, and Q.-K. Xue, *Science Bulletin* **61**, 1239 (2016).
- [31] J.-X. Yin, X.-X. Wu, J. Li, Z. Wu, J.-H. Wang, C.-S. Ting, P.-H. Hor, X. J. Liang, C. L. Zhang, P. C. Dai, X. C. Wang, C. Q. Jin, G. F. Chen, J. P. Hu, Z.-Q. Wang, A. Li, H. Ding, and S. H. Pan, *Phys. Rev. B* **102**, 054515 (2020).
- [32] F. Bernardini and A. Cano, *Journal of Physics: Materials* **3**, 03LT01 (2020).
- [33] B. Geisler and R. Pentcheva, *Phys. Rev. B* **102**, 020502 (2020).
- [34] R. He, P. Jiang, Y. Lu, Y. Song, M. Chen, M. Jin, L. Shui, and Z. Zhong, *Phys. Rev. B* **102**, 035118 (2020).
- [35] Q. Si and E. Abrahams, *Phys. Rev. Lett.* **101**, 076401 (2008).
- [36] K. Seo, B. A. Bernevig, and J. Hu, *Phys. Rev. Lett.* **101**, 206404 (2008).
- [37] K. Jiang, X. Wu, J. Hu, and Z. Wang, *Phys. Rev. Lett.* **121**, 227002 (2018).
- [38] Honerkamp, C., Wakabayashi, K., and Sigrist, M., *Europhys. Lett.* **50**, 368 (2000).
- [39] J. S. Hofmann, F. F. Assaad, and A. P. Schnyder, *Phys. Rev. B* **93**, 201116 (2016).
- [40] A. A. Golubov, M. Y. Kupriyanov, and E. Il'ichev, *Rev. Mod. Phys.* **76**, 411 (2004).
- [41] E. Goldobin, D. Koelle, R. Kleiner, and A. Buzdin, *Phys. Rev. B* **76**, 224523 (2007).
- [42] Z. Yang, S. Qin, Q. Zhang, C. Fang, and J. Hu, *Phys. Rev. B* **98**, 104515 (2018).
- [43] W.-C. Lee, S.-C. Zhang, and C. Wu, *Phys. Rev. Lett.* **102**, 217002 (2009).
- [44] Q. Gu, Y. Li, S. Wan, H. Li, W. Guo, H. Yang, Q. Li, X. Zhu, X. Pan, Y. Nie, and H.-H. Wen, arXiv e-prints , arXiv:2006.13123 (2020), [arXiv:2006.13123](https://arxiv.org/abs/2006.13123) [cond-mat.supr-con].
- [45] Y. Zhang, L.-F. Lin, W. Hu, A. Moreo, S. Dong, and E. Dagotto, arXiv e-prints , arXiv:2008.04392 (2020), [arXiv:2008.04392](https://arxiv.org/abs/2008.04392) [cond-mat.str-el].
- [46] G. Kresse and J. Hafner, *Phys. Rev. B* **47**, 558 (1993).
- [47] G. Kresse and J. Furthmüller, *Computational Materials Science* **6**, 15 (1996).
- [48] G. Kresse and J. Furthmüller, *Phys. Rev. B* **54**, 11169 (1996).
- [49] J. P. Perdew, K. Burke, and M. Ernzerhof, *Phys. Rev. Lett.* **77**, 3865 (1996).
- [50] H. J. Monkhorst and J. D. Pack, *Phys. Rev. B* **13**, 5188 (1976).

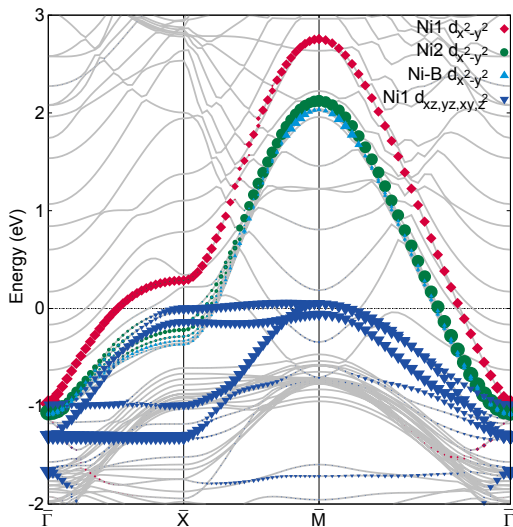


FIG. S5. (color online) DFT Band structure for NiO₂ terminated surface of NdNiO₂ without relaxation.

DETAILS OF DFT CALCULATIONS

Our DFT calculations employ the projector augmented wave (PAW) method encoded in the Vienna *ab initio* simulation package (VASP)[S46–S48], and the generalized-gradient approximation (GGA)[S49] for the exchange correlation functional are used. The cutoff energy of 500 eV is taken for expanding the wave functions into plane-wave basis and the Nd 4*f* electrons are considered frozen in the core. In calculations for both nickelates and cuprates, we modeled the surfaces using a slab of eight NiO₂/CuO₂ layers and eight or nine Nd/Ca layers plus a vacuum layer of 15 Å. The number of layers is large enough to give converged electronic structures of surface layers. The adopted lattice parameters are $a = 3.91$ Å and $c = 3.37$ Å for NdNiO₂ and $a = 3.86$ Å and $c = 3.20$ Å for CaCuO₂. The Brillouin zone is sampled in the k space within the Monkhorst-Pack scheme[S50]. The number of these k points is $9 \times 9 \times 1$ for two terminations of NdNiO₂ and CaCuO₂. In the relaxation, the bottom five layers are fixed while the others are allowed to move freely and forces are minimized to less than 0.02 eV/Å. We have checked the dipole correction on the atomic relaxation and find that it has negligible effect. After relaxation, one prominent feature is that surface NiO₂/CuO₂ layers are not planar and buckled in both terminations, distinct from bulk layers.

For NiO₂ terminated surface without relaxation, the band structure is shown in Fig.S5. For the surface NiO₂ layer, we find that besides the hole pocket around the $\bar{\Gamma}$ point, there are Fermi surfaces around M point attributed to $d_{xz/yz}$ and d_{xy} orbitals for the surface layer. After relaxation, the lattice distortions push these bands below the Fermi level (see the main text) but Fermi surface around the M point can still appear in hole-doped nickelates (Nd,Sr)NiO₂. To demonstrate it, we study Sr doped nickelates Nd_{0.8}Sr_{0.2}NiO₂ using the virtual

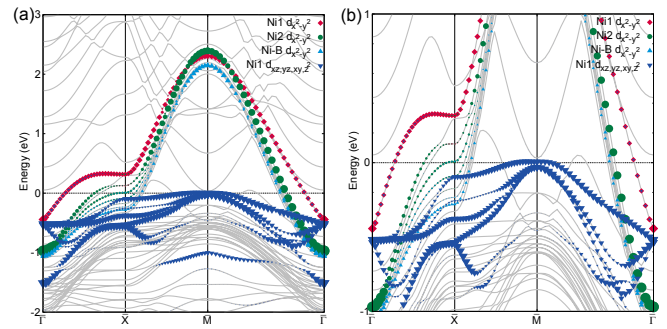


FIG. S6. (color online) (a) DFT Band structure for NiO₂ terminated surface of Nd_{0.8}Sr_{0.2}NiO₂ with relaxation. (b) A zoom-in band structure. Besides the electron pocket around $\bar{\Gamma}$, there is a hole pocket around \bar{M} .

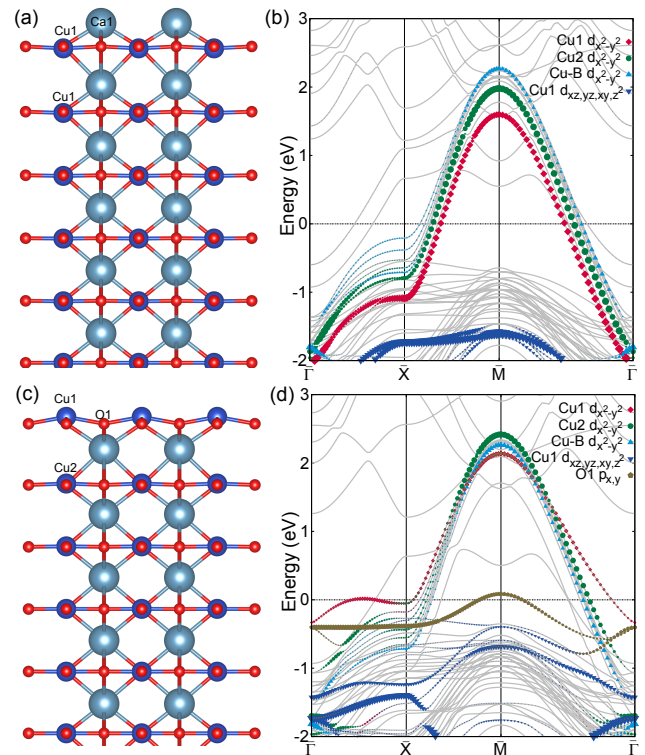


FIG. S7. (color online) (a) Crystal structures for Ca terminated (a) and CuO₂ terminated (c) surfaces of CaCuO₂. The corresponding orbital resolved band structures are in (b) and (d). "Ni-B" denotes the bulk Ni atom.

crystal approximation in DFT calculations and the band structure is displayed in Fig.S6. There is an additional hole pocket around M point, attributed to $d_{xz/yz}$ and d_{xy} orbitals. This is consistent with the doping using a rigid-band shift of the Fermi level in our tight-binding model in the main text.

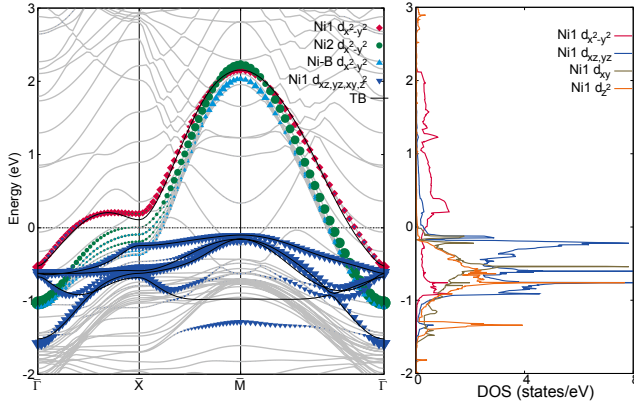


FIG. S8. (color online) Band structure from DFT and five-band tight-binding model (black lines) for NiO_2 terminated surface and orbitally resolved DOS for the Ni1 atom.

TABLE I. Calculated on-site energies relative to the $d_{x^2-y^2}$ orbital and hoppings of $d_{x^2-y^2}$ orbitals for surface and bulk NiO_2 layer in NdNiO_2 .

Wannier onsite energies (eV)	bulk layer	surface layer
$d_{xz/yz}$	-1.48	-1.03
d_{xy}	-1.38	-1.22
d_{z^2}	-1.73	-1.32
hoppings of $d_{x^2-y^2}$ orbital (eV)		
t_x	-0.3761	-0.3369
t_{xy}	0.0844	0.0889
t_{xx}	-0.0414	-0.0329

BAND STRUCTURE FOR CuO_2 AND CA TERMINATED SURFACES IN CaCuO_2

To demonstrate the unique features of surface NiO_2 layers, we also performed calculations for CuO_2 and Ca terminated surfaces in a typical infinite-layer cuprate CaCuO_2 . Similar to nickelates, the surface CuO_2 is buckled in both terminations, as shown in Fig.S7 (a) and (c). For Ca terminated surface, the band structure is displayed in Fig.S7 (b) and the surface layer is electron doped, similar with nickelates. From the orbitally resolved band structure of the CuO_2 terminated surface in Fig.S7 (d), the surface layer is heavily hole doped and there is an additional hole pocket attributed to oxygen atoms, indicating that the holes are located at oxygen sites. This is consistent with the charge-transfer nature of cuprates and other Cu d orbitals are well below the Fermi level. These features are in sharp contrast to the case of nickelates, where multi-orbital nature is essential for the surface NiO_2 layer. Therefore, the

surface pairing propensity in infinite-layer nickelates is quite intriguing.

TIGHT-BINDING MODELS OF THE SURFACE NiO_2 LAYER IN ND TERMINATED AND NiO_2 TERMINATED SURFACES

For Nd terminated surface, the electronic structure is dominated by the Ni $d_{x^2-y^2}$ orbital and therefore can be described by a one-band tight-binding model. The Hamiltonian matrix can be written as,

$$\begin{aligned}
 h_{Nd}(\mathbf{k}) = & \epsilon_0 - \mu + 2s_{11}^x(\cos k_x + \cos k_y) + 4s_{11}^{xy}\cos k_x\cos k_y \\
 & + 2s_{11}^{xx}(\cos 2k_x + \cos 2k_y) \\
 & + 4s_{11}^{xy}(\cos 2k_x\cos k_y + \cos k_x\cos 2k_y) \\
 & + 4s_{11}^{xxyy}\cos 2k_x\cos 2k_y,
 \end{aligned} \tag{S5}$$

with hopping parameters

$$\begin{aligned}
 s_{11}^x = -0.316575, \quad s_{11}^{xy} = 0.092113, \quad s_{11}^{xx} = -0.047588, \\
 s_{11}^{xxy} = -0.004311, \quad s_{11}^{xxyy} = 0.003844, \quad \epsilon_0 = 3.283151,
 \end{aligned} \tag{S6}$$

in units of eV. The chemical potential for Nd terminated surfaces of NdNiO_2 and $\text{Nd}_{0.8}\text{Sr}_{0.2}\text{NiO}_2$ are $\mu = 3.1510$ eV and $\mu = 2.9710$ eV, respectively.

As discussed in the main text, the surface NiO_2 is heavily hole-doped and the corresponding Fermi surfaces are attributed to d_{xy} and $d_{xz/yz}$ orbitals besides $d_{x^2-y^2}$ orbitals, indicating that a multi-orbital TB model is required to capture the electronic structure. The onsite energies of Ni d orbitals in the surface layer is given in Table I, in comparison to bulk layers. We find that the relative onsite energies of d orbitals relative to $d_{x^2-y^2}$ orbital increase, originating from the absence of rare-earth atoms on the surface. We introduce the operator $\psi_{\mathbf{k}\sigma}^\dagger = [c_{1\sigma}^\dagger(\mathbf{k}), c_{2\sigma}^\dagger(\mathbf{k}), c_{3\sigma}^\dagger(\mathbf{k}), c_{4\sigma}^\dagger(\mathbf{k}), c_{5\sigma}^\dagger(\mathbf{k})]$, where $c_{\alpha\sigma}^\dagger(\mathbf{k})$ is a Fermionic creation operator with σ and α being spin and orbital indices, respectively. The orbital index $\alpha = 1, 2, 3, 4, 5$ represent the Ni $d_{x^2-y^2}$ for 1, d_{xy} for 2, d_{xz} for 3, d_{yz} for 4 and d_{z^2} for 5, respectively. The tight-binding Hamiltonian can be written as,

$$H_0 = \sum_{\mathbf{k}\sigma} \psi_{\mathbf{k}\sigma}^\dagger (h(\mathbf{k}) - \mu) \psi_{\mathbf{k}\sigma}. \tag{S7}$$

The matrix elements in the Hamiltonian $h(\mathbf{k})$ matrix are given by,

$$h_{11}(\mathbf{k}) = \epsilon_1 + 2t_{11}^x(\cos k_x + \cos k_y) + 4t_{11}^{xy}\cos k_x \cos k_y + 2t_{11}^{xx}(\cos 2k_x + \cos 2k_y) + 4t_{11}^{xy}(\cos 2k_x \cos k_y + \cos k_x \cos 2k_y) + 4t_{11}^{xyy}\cos 2k_x \cos 2k_y \quad (\text{S8})$$

$$h_{22}(\mathbf{k}) = \epsilon_2 + 2t_{22}^x(\cos k_x + \cos k_y) + 4t_{22}^{xy}\cos k_x \cos k_y + 2t_{22}^{xx}(\cos 2k_x + \cos 2k_y) + 4t_{22}^{xy}(\cos 2k_x \cos k_y + \cos k_x \cos 2k_y) + 4t_{22}^{xyy}\cos 2k_x \cos 2k_y \quad (\text{S9})$$

$$h_{33/44}(\mathbf{k}) = \epsilon_3 + 2t_{33}^x \cos k_{x/y} + 2t_{33}^y \cos k_{y/x} + 4t_{33}^{xy} \cos k_x \cos k_y + 2t_{33}^{xx} \cos 2k_{x/y} + 2t_{33}^{yy} \cos 2k_{y/x} + 4t_{33}^{xy} \cos 2k_{x/y} \cos k_{y/x} + 4t_{33}^{xy} \cos k_{x/y} \cos 2k_{y/x} \quad (\text{S10})$$

$$h_{55}(\mathbf{k}) = \epsilon_5 + 2t_{55}^x(\cos k_x + \cos k_y) + 4t_{55}^{xy}\cos k_x \cos k_y + 2t_{55}^{xx}(\cos 2k_x + \cos 2k_y) + 4t_{55}^{xy}(\cos 2k_x \cos k_y + \cos k_x \cos 2k_y) + 4t_{55}^{xyy}\cos 2k_x \cos 2k_y \quad (\text{S11})$$

$$h_{12}(\mathbf{k}) = -4t_{12}^{xy}(\sin 2k_x \sin k_y - \sin k_x \sin 2k_y), \quad (\text{S12})$$

$$h_{13/14}(\mathbf{k}) = \pm 2it_{13}^x \sin k_{x/y} \pm 4it_{13}^{xy} \sin k_{x/y} \cos k_{y/x}, \quad (\text{S13})$$

$$h_{15}(\mathbf{k}) = 2t_{15}^x(\cos k_x - \cos k_y) + 2t_{15}^{xx}(\cos 2k_x - \cos 2k_y) + 4t_{15}^{xy}(\cos 2k_x \cos k_y - \cos k_x \cos 2k_y), \quad (\text{S14})$$

$$h_{23/24}(\mathbf{k}) = 2it_{23}^y \sin k_{y/x} + 4it_{23}^{xy} \cos k_{x/y} \sin k_{y/x} + 4it_{23}^{xy} \cos 2k_{x/y} \sin k_{y/x}, \quad (\text{S15})$$

$$h_{25}(\mathbf{k}) = -4t_{25}^{xy} \sin k_x \sin k_y - 4t_{25}^{xx}(\sin 2k_x \sin k_y - \sin k_x \sin 2k_y), \quad (\text{S16})$$

$$h_{34}(\mathbf{k}) = -4t_{34}^{xy} \sin k_x \sin k_y, \quad (\text{S17})$$

$$h_{35/45}(\mathbf{k}) = 2it_{35}^x \sin k_{x/y} + 4it_{35}^{xy} \sin k_{x/y} \cos k_{y/x} + 2it_{35}^{xx} \sin 2k_{x/y}. \quad (\text{S18})$$

The corresponding tight binding parameters are specified in unit of eV as,

$$\epsilon_1 = 2.824439, \quad \epsilon_2 = 1.602385, \quad \epsilon_3 = 1.794899, \quad \epsilon_5 = 1.503426, \quad (\text{S19})$$

$$t_{11}^x = -0.336882, \quad t_{11}^{xy} = 0.088921, \quad t_{11}^{xx} = -0.032852, \quad t_{11}^{xyy} = 0.0, \quad t_{11}^{xyy} = 0.004716, \quad (\text{S20})$$

$$t_{22}^x = -0.161413, \quad t_{22}^{xy} = -0.027797, \quad t_{22}^{xx} = -0.007141, \quad t_{22}^{xyy} = -0.007962, \quad t_{22}^{xyy} = -0.004822,$$

$$t_{33}^x = -0.107864, \quad t_{33}^y = -0.014042, \quad t_{33}^{xy} = 0.005590, \quad t_{33}^{xx} = 0.022678, \quad t_{33}^{yy} = t_{33}^{xyy} = t_{33}^{xyy} = 0,$$

$$t_{55}^x = 0.038130, \quad t_{55}^{xy} = -0.018292, \quad t_{55}^{xx} = t_{55}^{yy} = t_{55}^{xy} = t_{55}^{xyy} = 0,$$

$$t_{12}^{xy} = 0.008613, \quad t_{13}^x = -0.231015, \quad t_{13}^{xy} = 0.015815, \quad t_{15}^x = -0.011937, \quad t_{15}^{xx} = -0.003796$$

$$t_{15}^{xy} = 0, \quad t_{23}^y = -0.009767, \quad t_{23}^{xy} = 0.016265, \quad t_{23}^{xyy} = 0.007045, \quad t_{25}^{xy} = 0.004568$$

$$t_{25}^{xyy} = 0, \quad t_{34}^{xy} = 0.016076, \quad t_{35}^x = -0.101877, \quad t_{35}^{xy} = 0.008791, \quad t_{35}^{xx} = 0. \quad (\text{S21})$$

Without Sr doping, the chemical potential is $\mu = 2.2519$ eV with the occupation number being 8.2. With the above parameters, the obtained band structures (black lines) are shown in Fig.S8, in good agreement with DFT calculations (Ni1 orbitally resolved bands). Near the Fermi level, the DOS is dominantly attributed to $d_{x^2-y^2}$, d_{xy} and $d_{xz/yz}$ orbitals. For $\text{Nd}_{1-x}\text{Sr}_x\text{NiO}_2$ with $0.12 \leq x \leq 0.25$ in experiments, the hole doping for the surface NiO_2 layer is estimated to be $0.08 \leq \delta \leq 0.16$. For $\text{Nd}_{0.8}\text{Sr}_{0.2}\text{NiO}_2$, the corresponding chemical potential is $\mu = 2.1339$ eV with $\delta = 0.12$ and the corresponding Fermi surfaces are displayed in the main text.

MULTI-ORBITAL T-J MODEL FOR SURFACE NiO_2 LAYERS

In the strong-coupling limit, similar to iron based superconductors, we consider for the surface NiO_2 layers in-plane antiferromagnetic couplings between the Ni spins,

$$H_J = \sum_{\langle ij \rangle \alpha} J_{ij}^\alpha (\mathbf{S}_{i\alpha} \mathbf{S}_{j\alpha} - \frac{1}{4} n_{i\alpha} n_{j\alpha}) \quad (\text{S22})$$

where $\mathbf{S}_{i\alpha} = \frac{1}{2} c_{i\alpha\sigma}^\dagger \boldsymbol{\sigma}_{\sigma\sigma'} c_{i\alpha\sigma'}$ is the local spin operator and $n_{i\alpha}$ is the local density operator for Ni α orbital ($\alpha = x^2 - y^2, xy, xz, yz, z^2$). $\langle ij \rangle$ denotes the in-plane nearest neighbors and the in-plane coupling is $J_x^\alpha = J_y^\alpha = J_1^\alpha$. By performing the Fourier transformation, H_J in momentum space reads

$$H_J = \sum_{\alpha\mathbf{k}, \mathbf{k}'} V_{\mathbf{k}, \mathbf{k}'}^\alpha c_{\mathbf{k}\alpha\uparrow}^\dagger c_{-\mathbf{k}\alpha\downarrow}^\dagger c_{-\mathbf{k}'\alpha\downarrow} c_{\mathbf{k}'\alpha\uparrow}, \quad (\text{S23})$$

with $V_{\mathbf{k}, \mathbf{k}'}^\alpha = -\frac{2J_1^\alpha}{N} \sum_{\pm} (\cos k_x \pm \cos k_y)(\cos k'_x \pm \cos k'_y)$. Here we investigate the pairing state for doped system and neglect the no-double-occupancy constraint on this $t - J$ model and perform a mean-field decoupling. With this, the total Hamiltonian can be written as,

$$H_{MF} = \sum_{\mathbf{k}} \Psi_{\mathbf{k}}^\dagger A(\mathbf{k}) \Psi_{\mathbf{k}} + \sum_{\alpha; \nu=s,d} \frac{N}{2J_1^\alpha} |\Delta_\alpha^\nu|^2, \quad (\text{S24})$$

$$A(\mathbf{k}) = \begin{pmatrix} h(\mathbf{k}) & \Delta_{\uparrow\downarrow}(\mathbf{k}) \\ \Delta_{\uparrow\downarrow}^\dagger(\mathbf{k}) & -h^*(-\mathbf{k}) \end{pmatrix},$$

$$\Delta_{\uparrow\downarrow}(\mathbf{k}) = \text{diag}\{\Delta_1(\mathbf{k}), \Delta_2(\mathbf{k}), \Delta_3(\mathbf{k}), \Delta_4(\mathbf{k}), \Delta_5(\mathbf{k})\}, \quad (\text{S25})$$

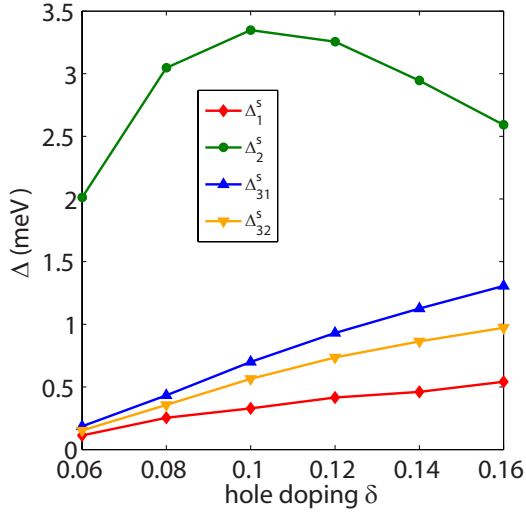


FIG. S9. (color online) Orbital dependent superconducting gaps as a function of hole doping for $J_1^1 = 0.12$ with $J_1^{2,3,4} = J_1^1/2$.

where $\Psi_{\mathbf{k}}^\dagger = (\psi_{\mathbf{k}\uparrow}^\dagger, \psi_{-\mathbf{k}\downarrow}^T)$, $\Delta_\alpha(\mathbf{k}) = \Delta_\alpha^s(\cos k_x + \cos k_y) + \Delta_\alpha^d(\cos k_x - \cos k_y)$, and

$$\Delta_\alpha^{s/d} = -\frac{2J_1^\alpha}{N} \sum_{\mathbf{k}'} d_{\mathbf{k}'\uparrow}^\alpha (\cos k'_x \pm \cos k'_y), \quad (\text{S26})$$

with $d_{\mathbf{k}'\uparrow}^\alpha = \langle c_{-\mathbf{k}'\alpha\downarrow} c_{\mathbf{k}'\alpha\uparrow} \rangle$. $A(\mathbf{k})$ can be diagonalized by a unitary transformation $U_{\mathbf{k}}$ with and the Bogoliubov quasiparticle eigenvalues $E_{m+5} = -E_m$ with $m = 1, 2, 3, 4, 5$. The

self-consistent gap equations are

$$\Delta_\alpha^{s/d} = -\frac{2J_1^\alpha}{N} \sum_{\mathbf{k}, m} (\cos k_x \pm \cos k_y) U_{\alpha+5, m}^*(\mathbf{k}) \times U_{\alpha, m}(\mathbf{k}) F[E_m(\mathbf{k})], \quad (\text{S27})$$

where $F[E]$ is Fermi-Dirac distribution function, $F[E] = 1/(1 + e^{E/k_B T})$. We further introduce $\Delta_{31}^{s/d} = \frac{1}{2}(\Delta_3^s \pm \Delta_4^s + \Delta_3^d \mp \Delta_4^d)$ and $\Delta_{32}^{s/d} = \frac{1}{2}(\Delta_3^s \pm \Delta_4^s - \Delta_3^d \pm \Delta_4^d)$ for $d_{xz/yz}$ orbitals. The above equations can be solved self-consistently, varying the doping and the value of J_1^α . In the calculations, we used $J_1^{2,3,4} = J_1^1/2$ and omitted the exchange coupling for d_{z^2} orbital i.e. $J_1^5 = 0$. The orbital dependent superconducting gaps as a function of hole doping is displayed in Fig.S9, where the extended s -wave pairing is always dominant and d_{xy} has the largest gap size.

With including interlayer couplings between the surface and bulk NiO₂ layers in NiO₂ terminated surface, we perform calculations to study pairing states. The electronic structure of bulk NiO₂ layers can be described by one-band model and we consider the Hamiltonian $H = H_0 + H_1 + H_t$, where H_1 describes the bulk layer with a hole pocket around \bar{M} and H_t is the tunneling between the two layers. In the calculations, the band structure of bulk NiO₂ layer is approximated by that at $k_z = 0$ plane and the corresponding parameters can be found in Ref.S11. For interlayer couplings, we include the nearest-neighbor (NN) coupling between $d_{x^2-y^2}$ orbitals in two layers $t_{16}^z = -0.0368$ eV and the fourth NN coupling between d_{xy} and $d_{x^2-y^2}$ orbitals in two layers $t_{26}^{xy} = 0.015$ eV (the NN to third NN hoppings vanish). By including the nearest neighbor exchange interactions for both layers, we solve the system within a mean-field decoupling similar to the case of surface layers and find the $s_\pm - id_{x^2-y^2}$ pairing state is energetically more favorable. We have further included two or three bulk NiO₂ layers in our calculations and find that $s_\pm - id_{x^2-y^2}$ is always favored.